Supporting Information

Revealing unusual temperature-dependent CO_2 adsorption trend and selective CO_2 uptake over water vapors in a polyamine-appended metal-organic framework

Jong Hyeak Choe,[a] Dong Won Kang,[a] Minjung Kang,[a] Hyojin Kim,[a] Jeoung Ryul Park,[a] Dae Won Kim,[a] and Chang Seop Hong[a]*

[a] *Department of Chemistry, Korea University, Seoul 02841, Republic of Korea.*

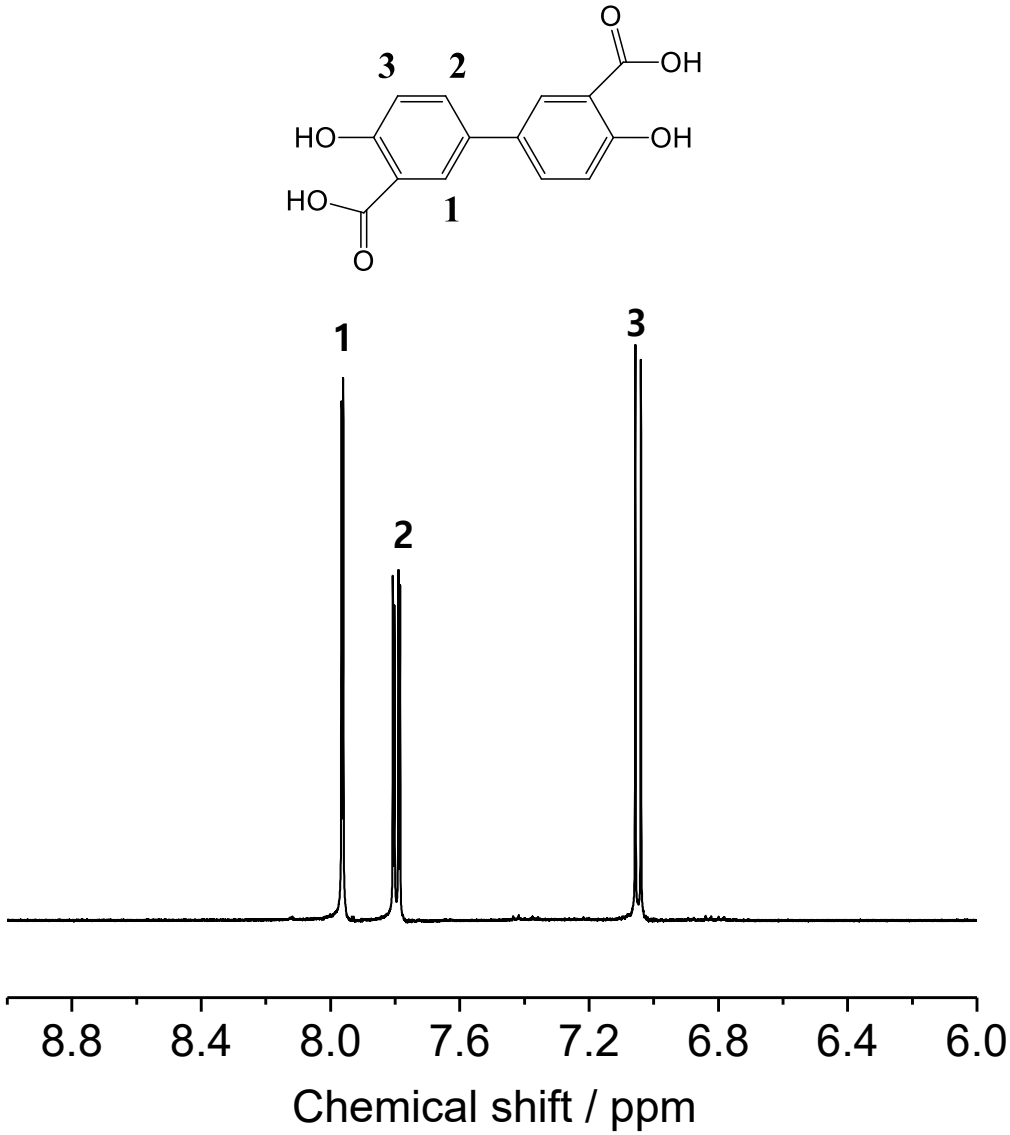

Fig. S1 ^{1}H NMR of H_4dobpdc (NMR solvent: DMSO-*d6*).

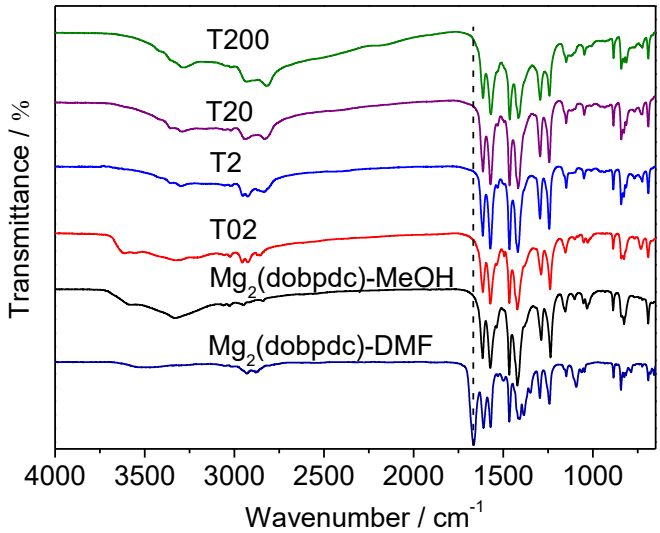

Fig. S2 FT-IR data of Mg_2(dobpdc)-DMF, Mg_2(dobpdc)-MeOH, and tepa-grafted samples.

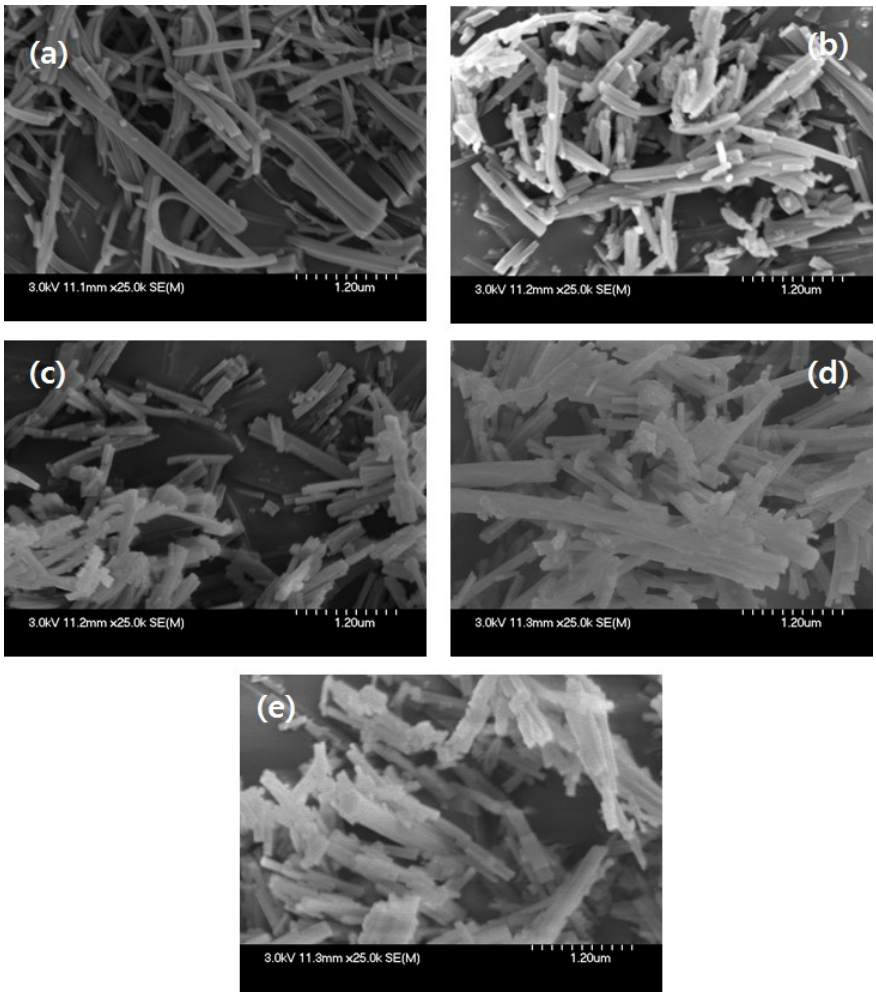

Fig. S3 SEM images of (a) Mg_2(dobpdc), (b) **T02**, (c) **T2**, (d) **T20**, and (e) **T200**.

(a)

XPS	Mg (%)	N (%)	O (%)	C (%)
T02	5.4	5.1	24.1	65.4
T2	3.8	14.1	18.7	63.5
T20	3.9	16.8	18.6	60.7
T200	3.5	18.2	17.3	60.8

(b)

Elemental analysis	N (%)	C (%)	H (%)
T02	1.98	49.20	4.39
T2	12.40	50.23	5.80
T20	14.35	49.90	6.67
T200	16.11	48.65	6.81

Table. S1 Composition of tepa-grafted MOFs through (a) XPS and (b) elemental analysis.

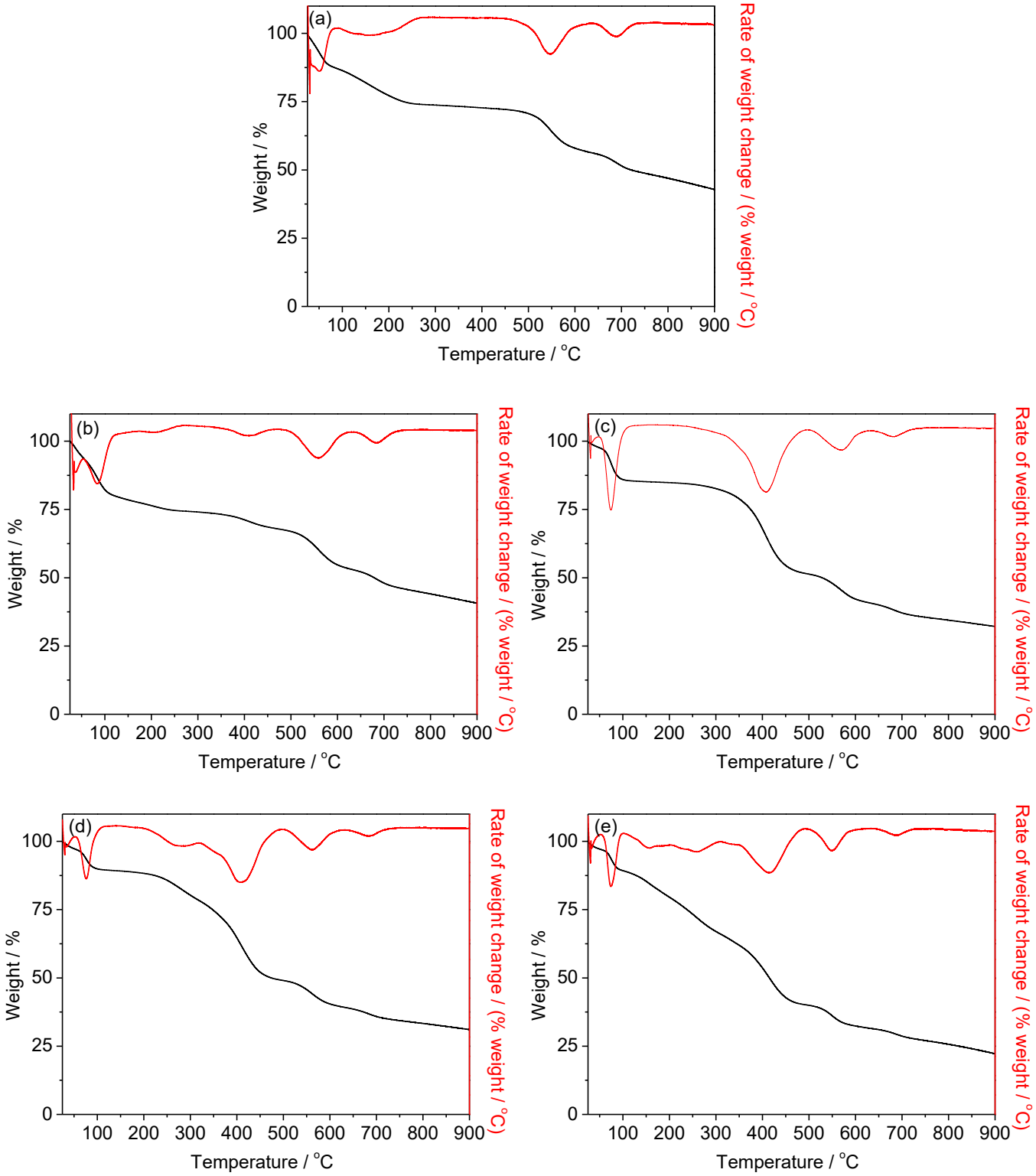

Fig. S4 Dry N_2 decomposition curves of (a) Mg_2(dobpdc), (b) **T02**, (c) **T2**, (d) **T20**, and (e) **T200**. A ramp rate was 3 °C/min.

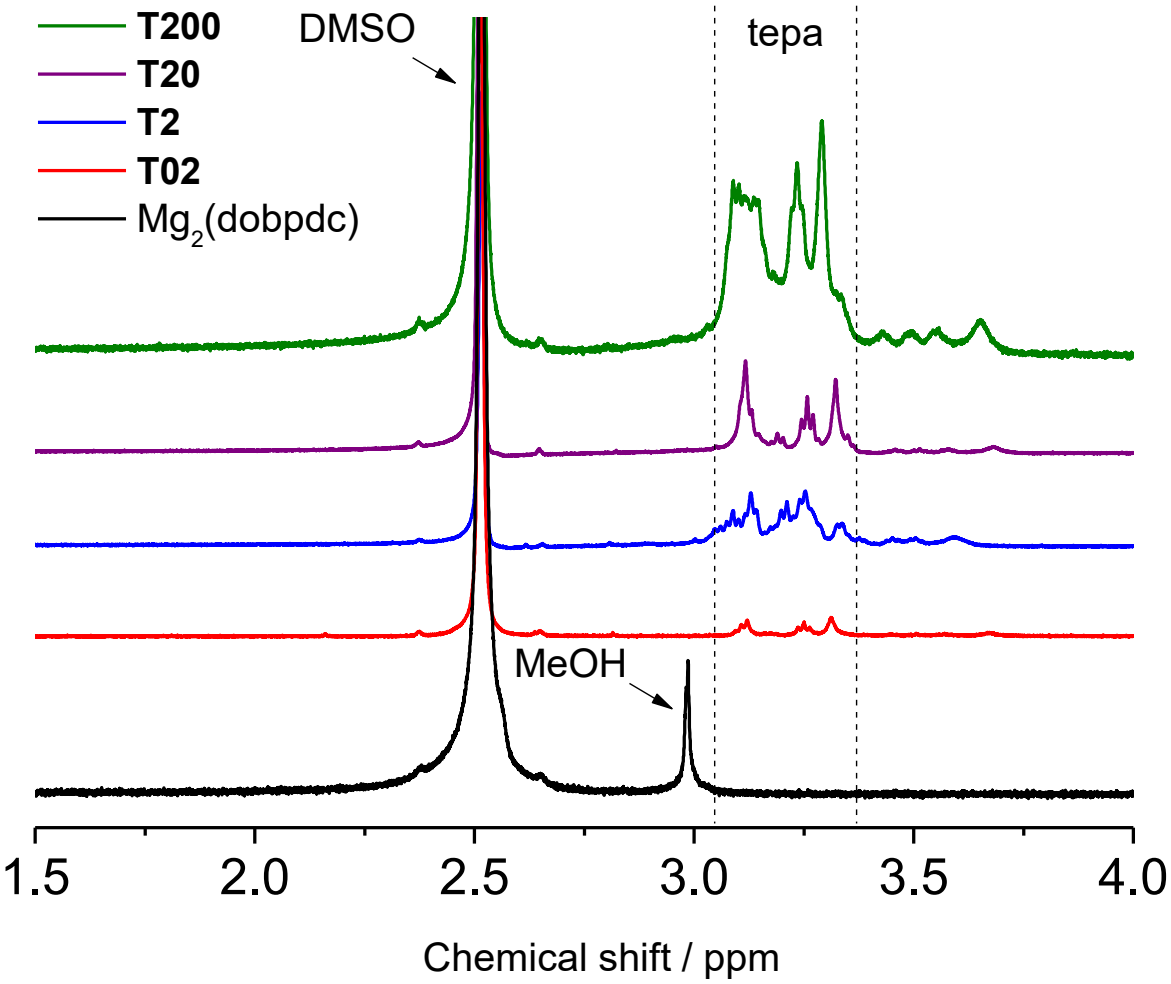

Fig. S5 Determination about tepa-loadings on MOFs (0.05 mmol) by ^{1}H NMR after digestion with DCl (35 wt% in D_2O) in DMSO-*d6*

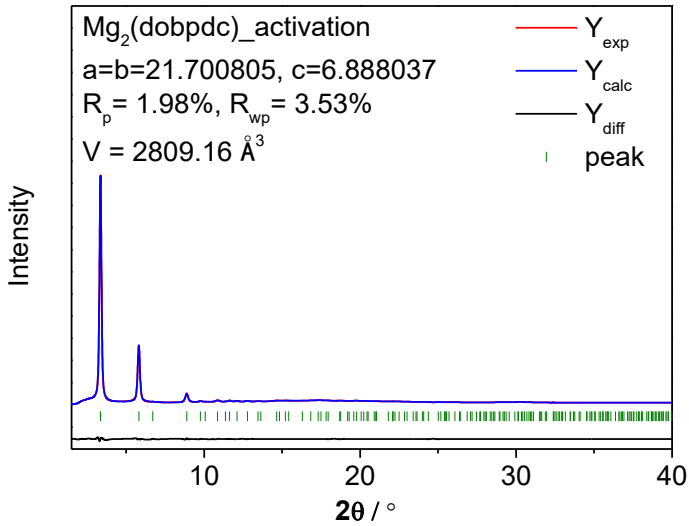

Fig. S6 Synchrotron powder X-ray diffraction pattern of Mg_2(dobpdc) with calculated diffraction pattern (blue) from Pawley refinement with difference (black).

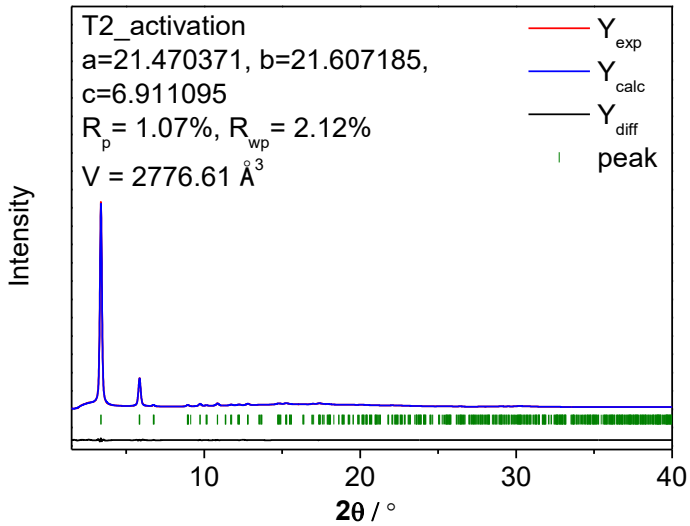

Fig. S7 Synchrotron powder X-ray diffraction pattern of **T2**-activated with calculated diffraction pattern (blue) from Pawley refinement with difference (black).

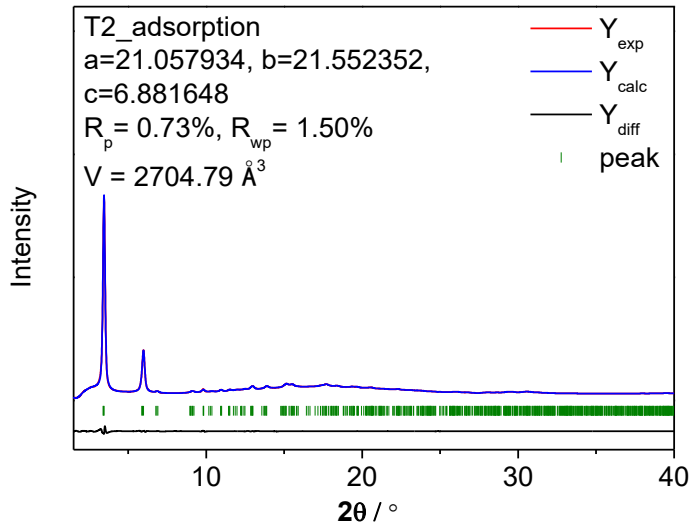

Fig. S8 Synchrotron powder X-ray diffraction pattern of **T2**-CO_2-captured with calculated diffraction pattern (blue) from Pawley refinement with difference (black).

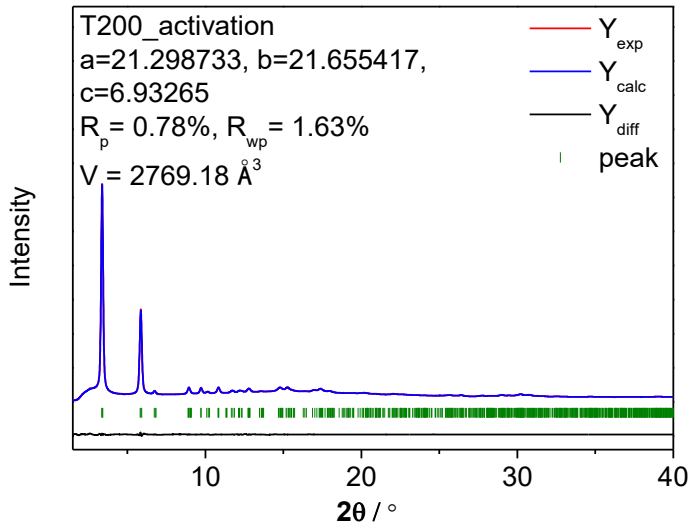

Fig. S9 Synchrotron powder X-ray diffraction pattern of **T200**-activated with calculated diffraction pattern (blue) from Pawley refinement with difference (black).

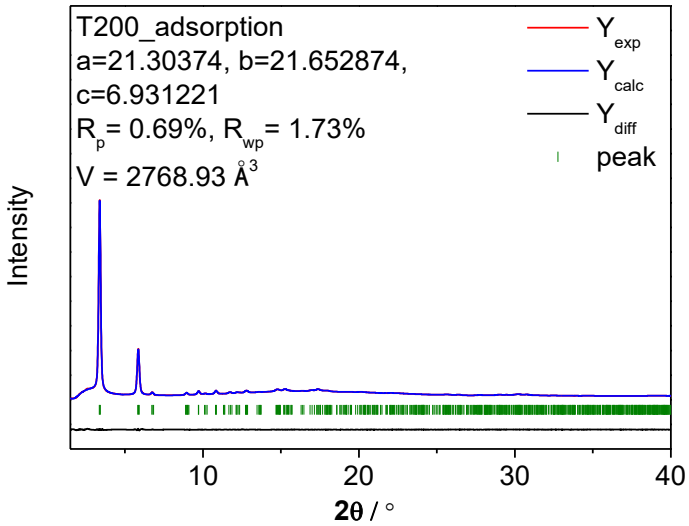

Fig. S10 Synchrotron powder X-ray diffraction pattern of **T200**-CO_2-captured with calculated diffraction pattern (blue) from Pawley refinement with difference (black).

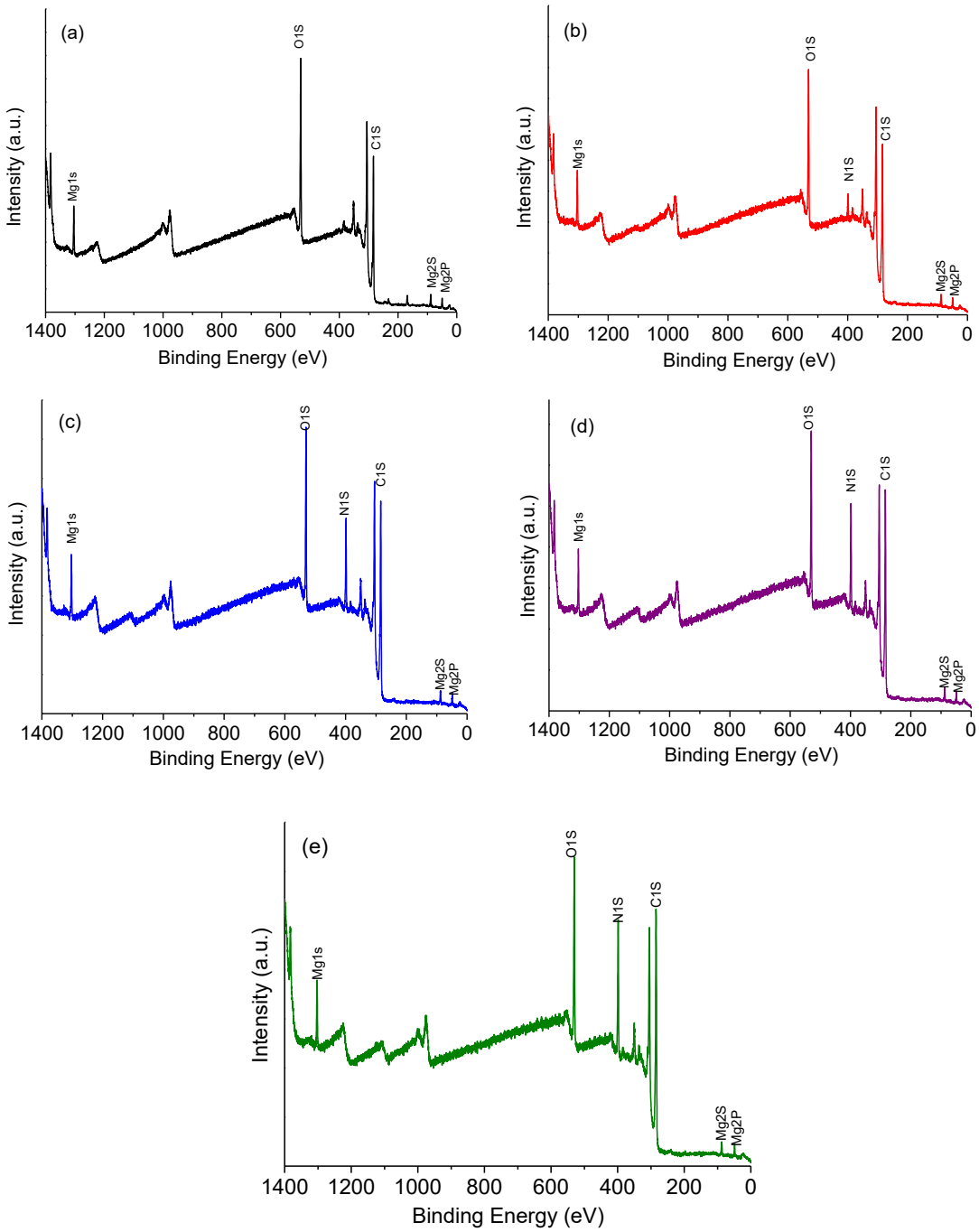

Fig. S11 Survey XPS scan for (a) Mg_2(dobpdc), (b) **T02**, (c) **T2**, (d) **T20**, and (e) **T200**.

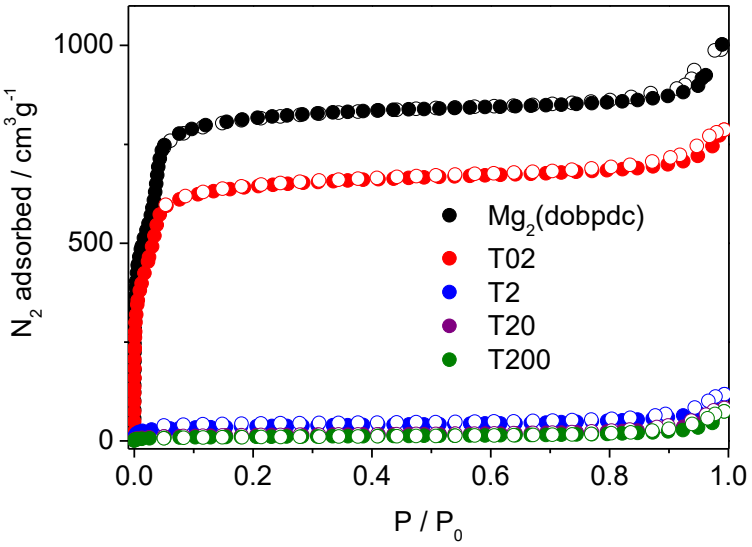

(a)

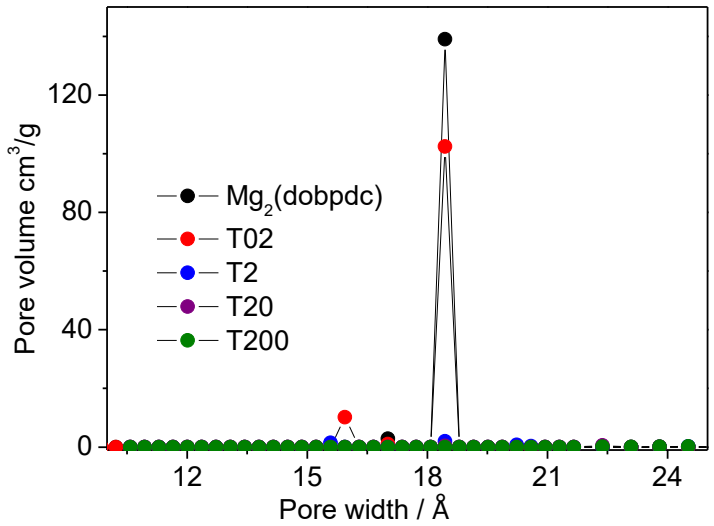

(b)

Fig. S12 N_2 adsorption isotherms of (a) Mg_2(dobpdc) and tepa-grafted MOFs at 77 K, and (b) DFT pore size distribution calculated from the N_2 adsorption at 77 K using cylindrical pores with oxide surface.

	S_{bet} (m^2/g)	S_L (m^2/g)	PV (cm^3/g) at 19.5 Å [a]
Mg_2(dobpdc)	3178	3743	138
T02	2372	2903	101
T2	131	175	2.07
T20	51	67	0.45
T200	36	48	0.03

[a] Micropore volume calculated from the nitrogen isotherm.

Table. S2 Porous proteries of Mg_2(dobpdc) and tepa-grafted MOFs.

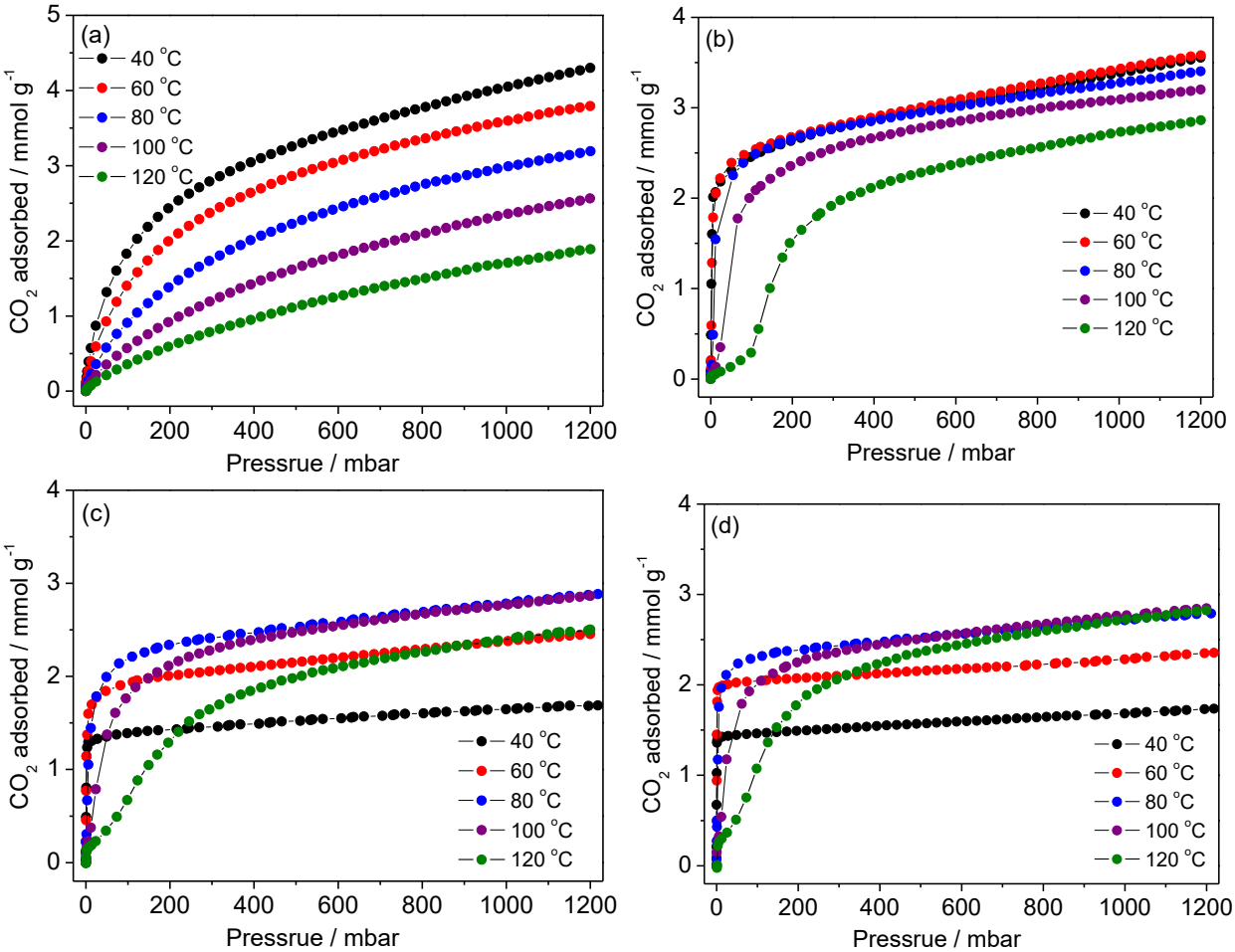

Fig. S13 Adsorption isotherms of CO_2 for (a) **T02**, (b) **T2**, (c) **T20**, and (d) **T200** on a linear scale. Measurement temperatures were indicated in the inset of the graph.

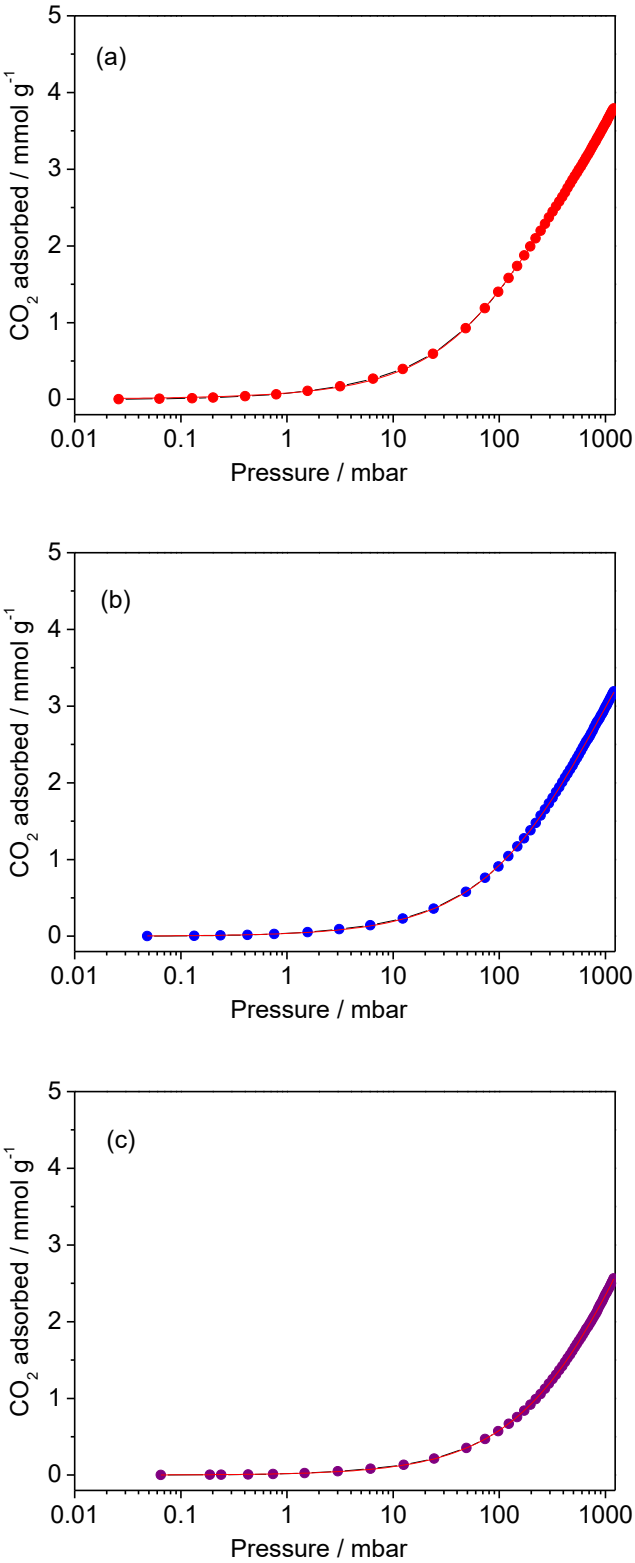

Fig. S14 CO_2 adsorption isotherms of **T02** at (a) 60 °C, (b) 80 °C, and (c) 100 °C, fitted by a dual-site Langmuir-Freundlich equation.

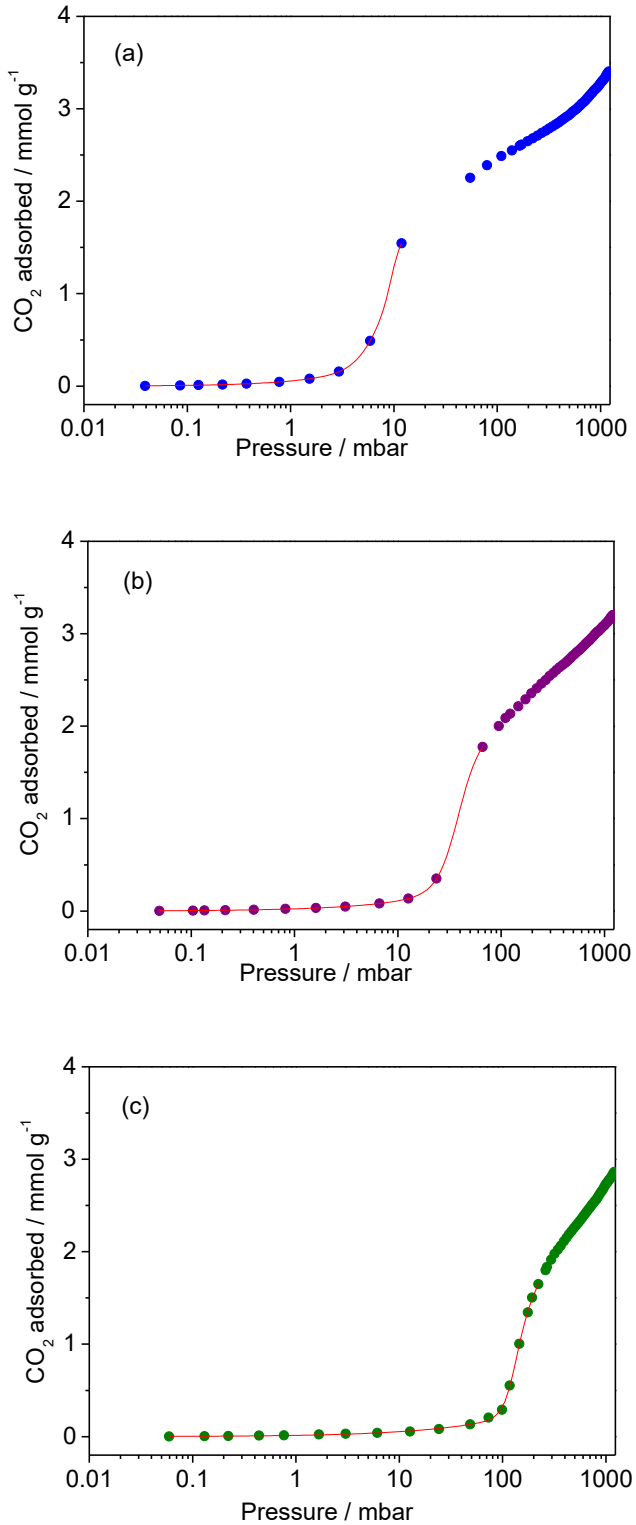

Fig. S15 CO_2 adsorption isotherms of **T2** at (a) 80 °C, (b) 100 °C, and (c) 120 °C, fitted by a dual-site Langmuir-Freundlich equation.

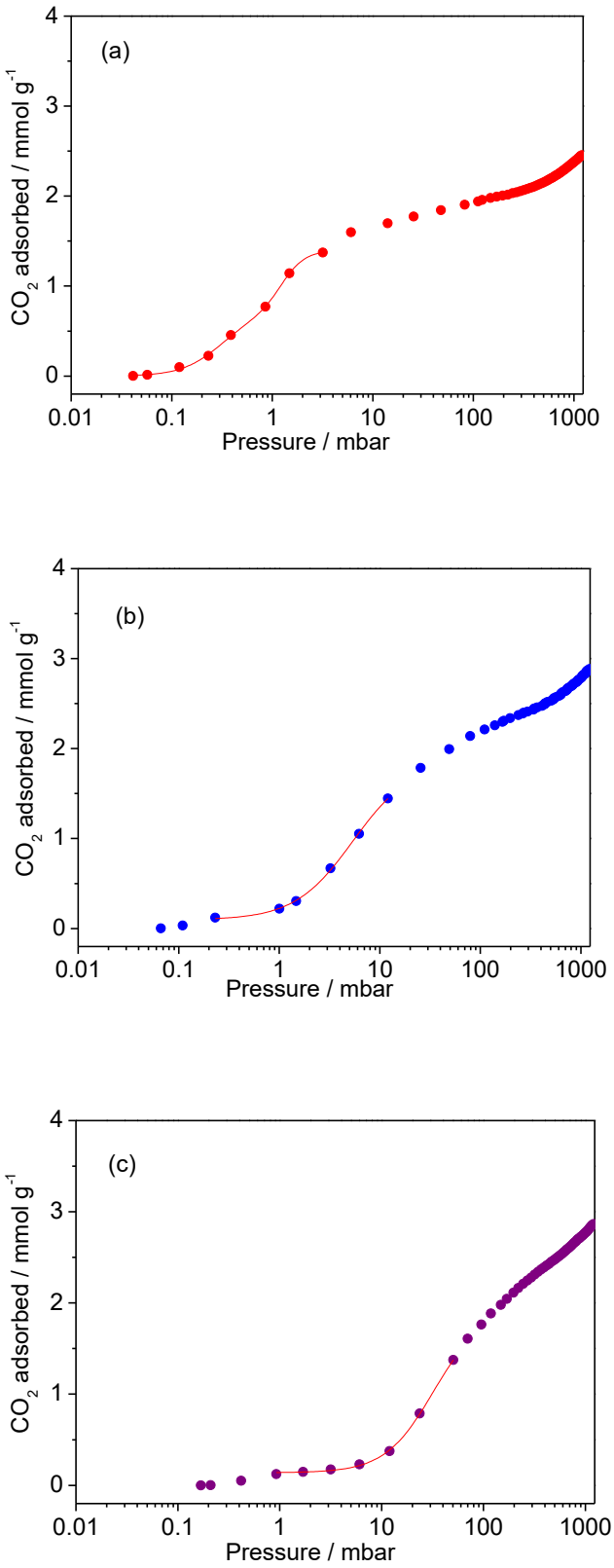

Fig. S16 CO_2 adsorption isotherms of **T20** at (a) 60 ºC, (b) 80 ºC, and (c) 100 ºC, fitted by a dual-site Langmuir-Freundlich equation.

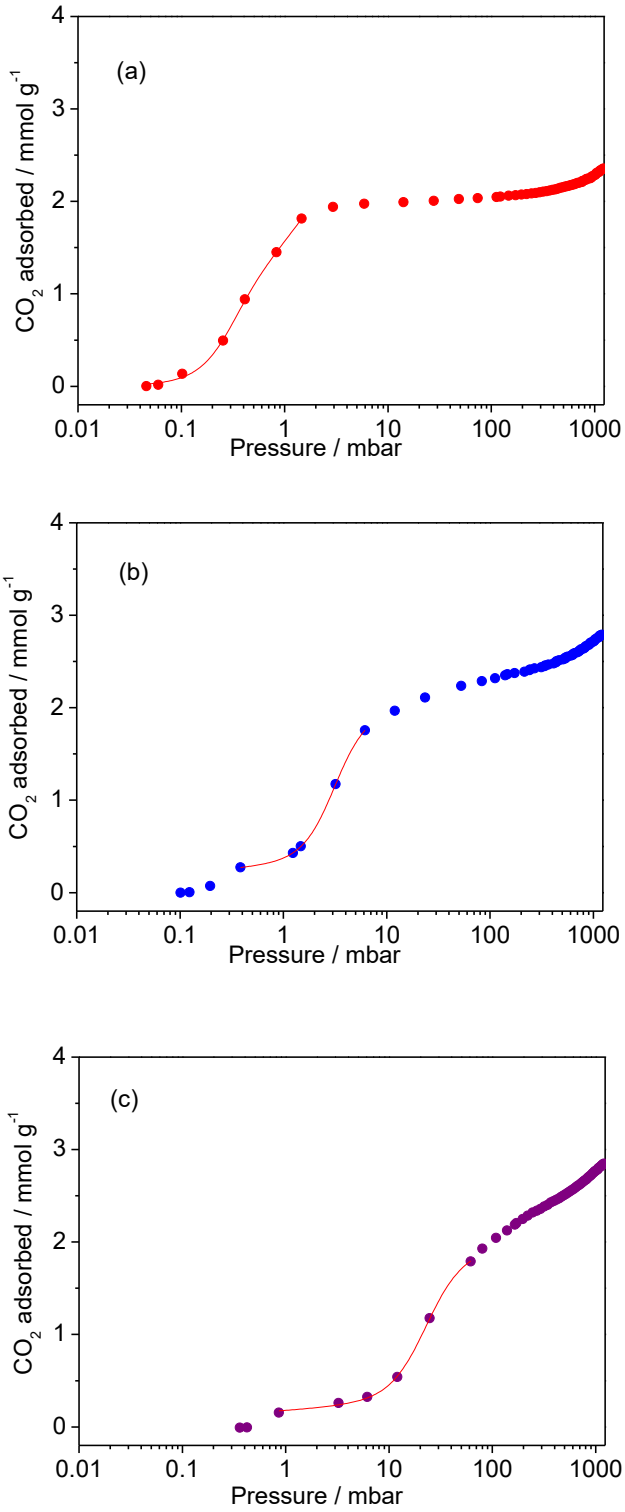

Fig. S17 CO_2 adsorption isotherms of **T200** at (a) 60 °C, (b) 80 °C, and (c) 100 °C, fitted by a dual-site Langmuir-Freundlich equation.

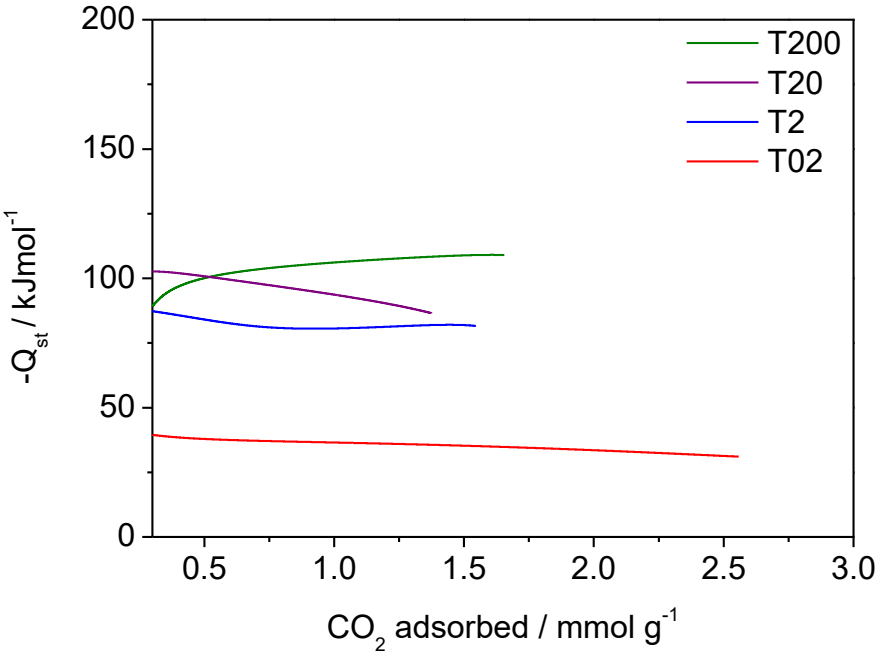

Fig. S18 Isosteric heats of CO_2 adsorption for **T02**, **T2**, **T20**, and **T200**, as calculated using the Clausius-Clapeyron relation.

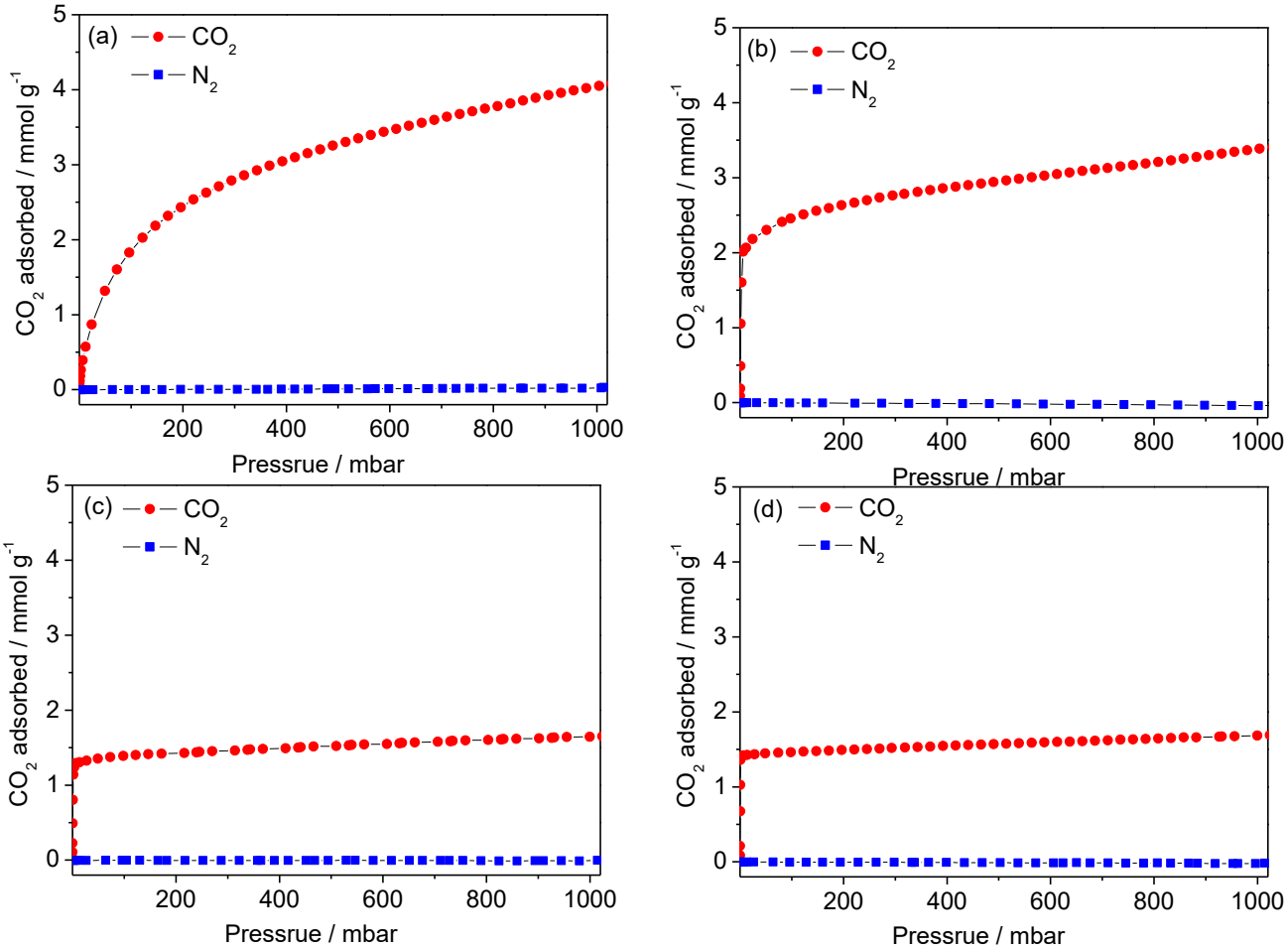

Fig S19 CO_2 and N_2 isotherms of (a) **T02**, (b) **T2**, (c) **T20**, and (d) **T200** at 40 °C.

	CO_2 uptake[a] (mmol/g)	N_2 uptake[b] (mmol/g)	Selectivity
T02	2.17	0.02	542
T2	2.53	0.01	1265
T20	1.43	0.006	1191
T200	1.46	0.007	1042

[a] CO_2 uptake determined 150 mbar and 40 °C. [b] N_2 uptake determined 750 mbar and 40 °C.

Table. S3 CO_2 and N_2 gas adsorptions of tepa-grafted MOFs.

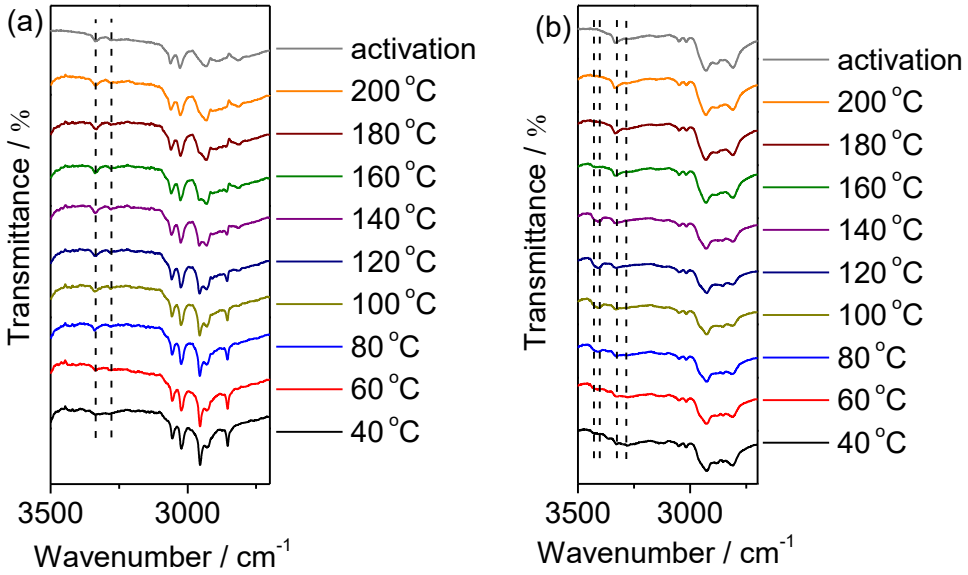

Fig. S20 In situ IR spectra of (a) **T02** and (b) **T20** showing N-H stretching vibrations. The IR data denote the peak changes over temperature under 100% CO_2.

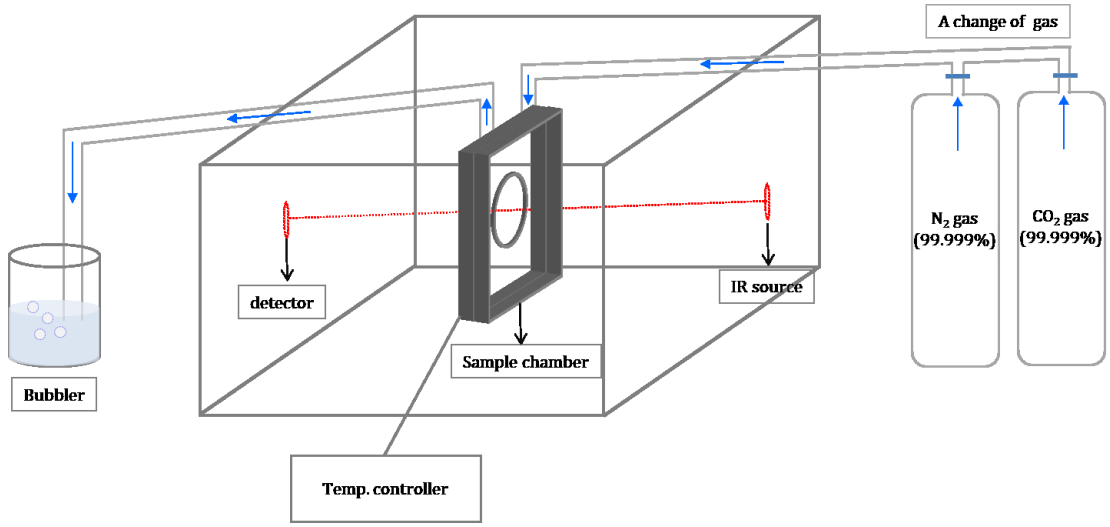

Fig. S21 A diagram of *in situ* infrared (IR) measurement.

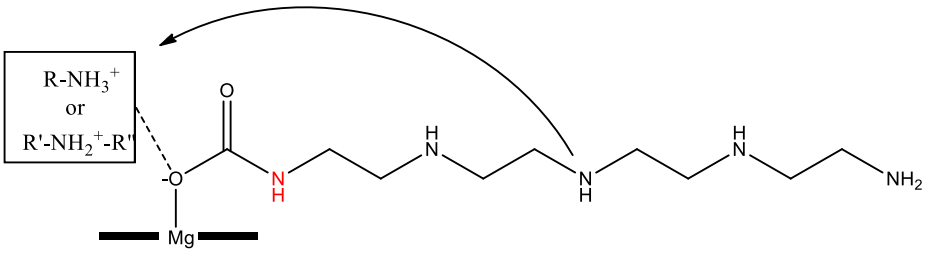

(a)

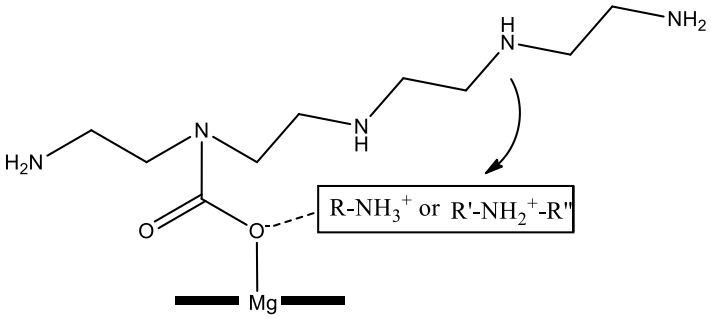

(b)

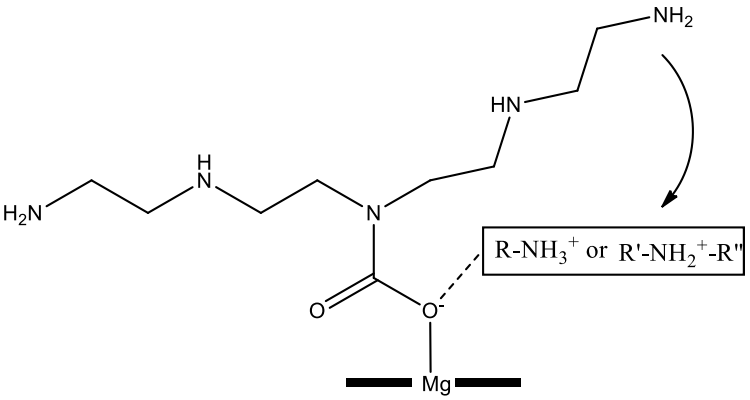

(c)

Fig. S22 Probable CO_2 adsorption modes. Carbamate N-H in red (a) is newly formed as a result of carbamate formation from primary amine group. No carbamate N-H group is generated when secondary amine group is involved in carbamate formation (b, c). Dotted lines indicate ion pairing between carbamate and ammonium species. Possible patterns of ammonium cations, generated by intra- or inter-amine group, are shown in the box. Amine groups of tepa that are located away from the carbamate group could serve as ammonium ions after abstracting protons from other amine groups (arrow: a, b, c).

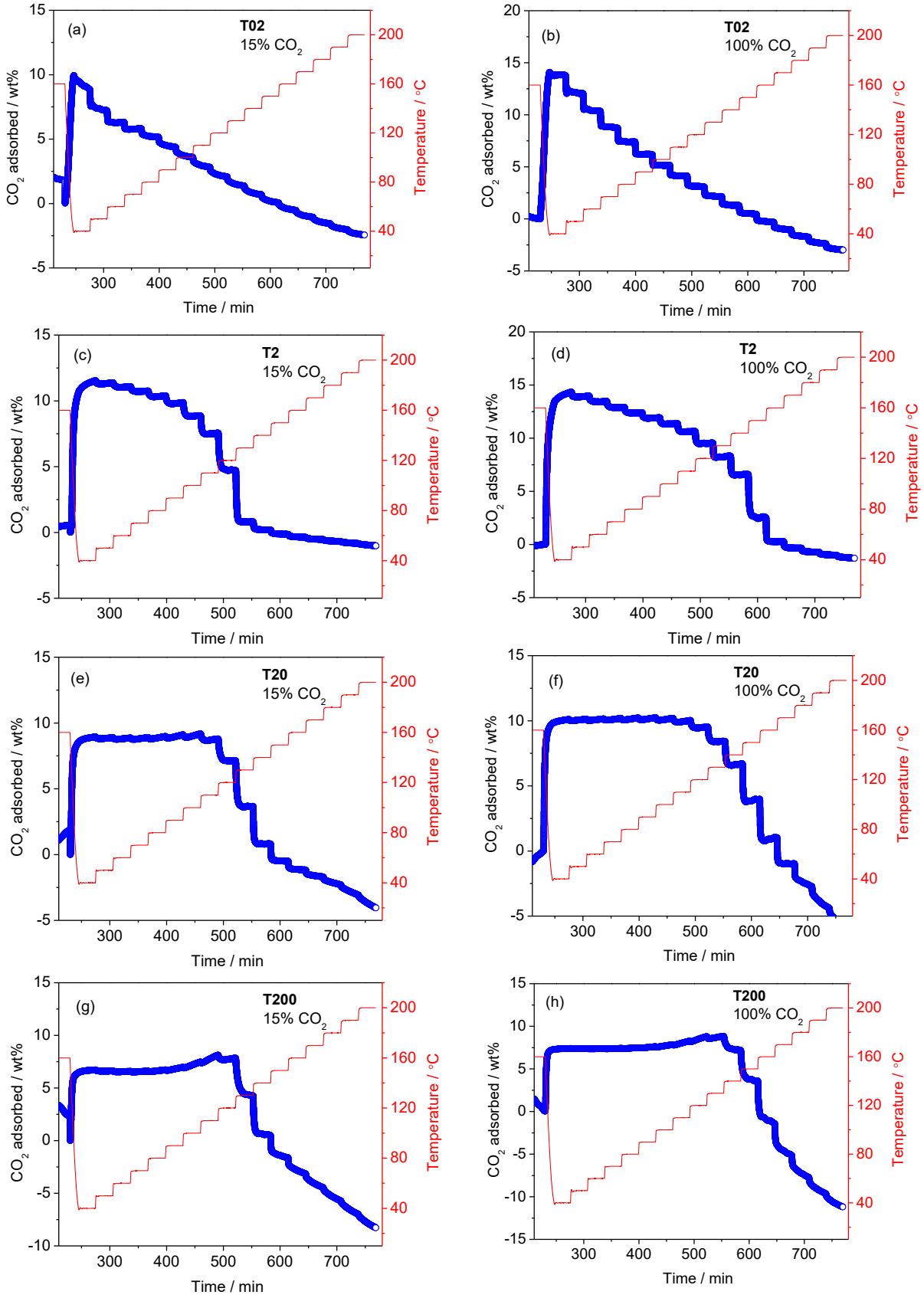

Fig. S23 Adsorption behaviors of tepa-appended Mg_2(dobpdc) at 15% and 100% CO_2.

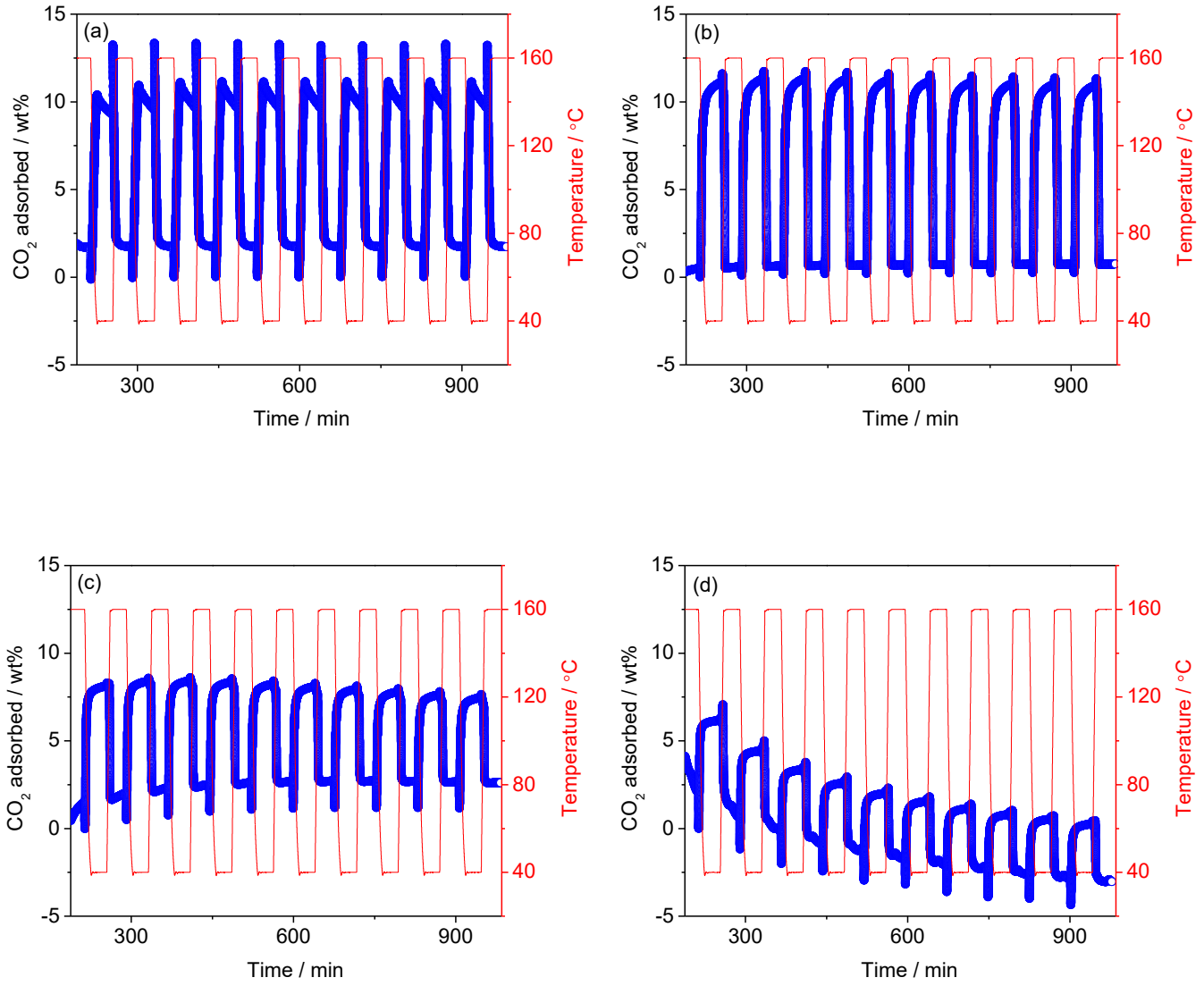

Fig. S24 Cyclic temperature-swing adsorption of (a) **T02**, (b) **T2**, (c) **T20**, and (d) **T200** Adsorption occurred at 40 ºC and 15% CO_2, while desorption happened at 100% CO_2 and 160 ºC.

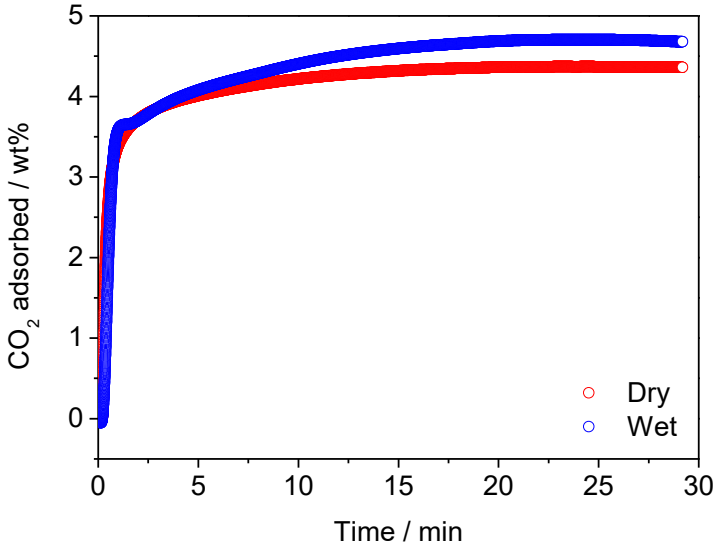

Fig. S25 Adsorption capacity of **T200** under dry (15% CO_2 and 85% He) and wet (15% CO_2, 3.75% H_2O, and 81.25% He) conditions. The flow rate of the mixed gas was 80 mL/min.

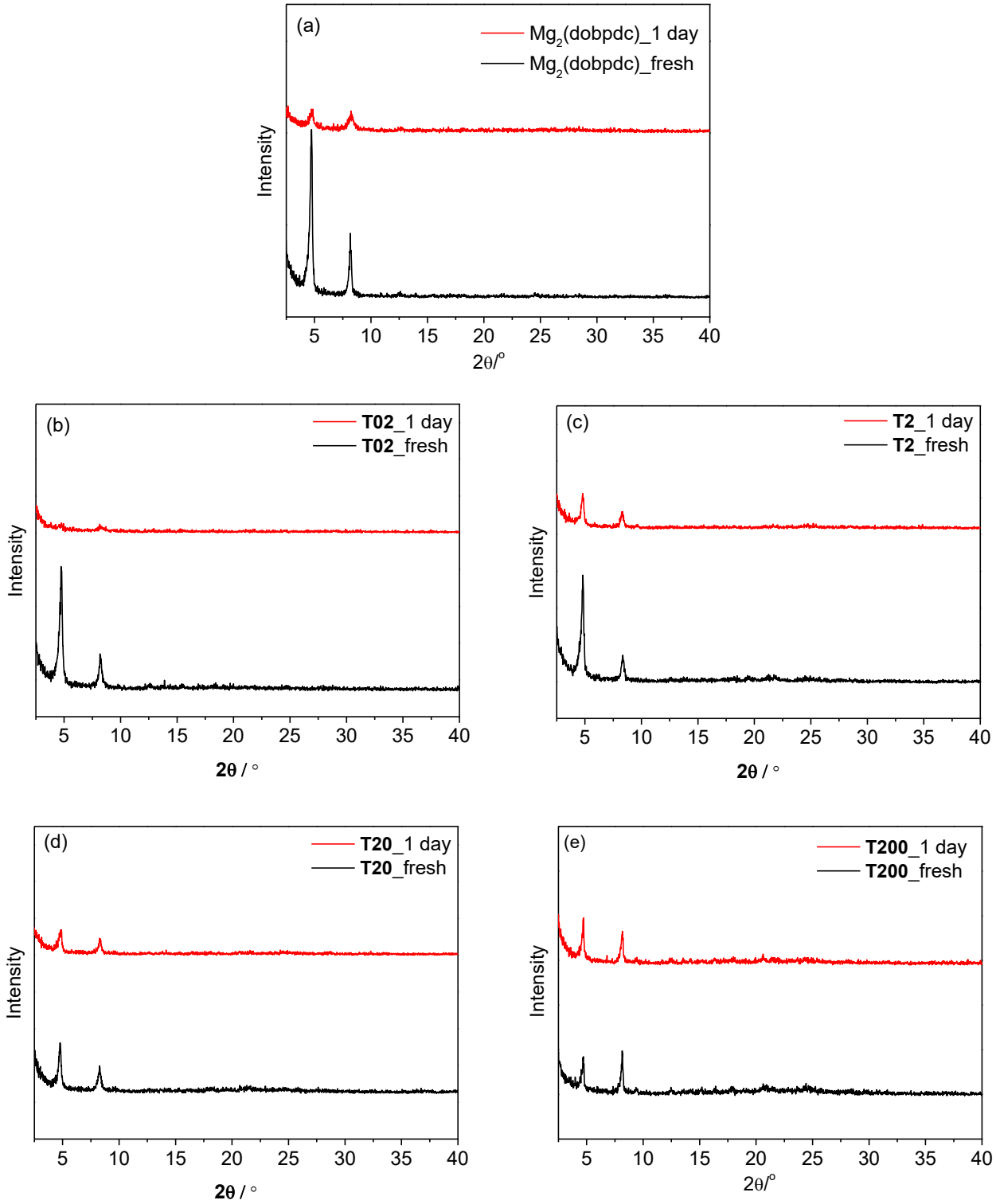

Fig. S26 PXRD profiles of (a) Mg_2(dobpdc), (b) **T02**, (c) **T2**, (d) **T20** and (e) **T200** before and after exposure to a mixture gas of 10% H_2O balanced by N_2 at 80 °C for 1 day.